Retrieval of Wind Wave Elevation Spectra From Sunglint Data

Geoff P. Cureton, Stuart J. Anderson, Mervyn J. Lynch, and Brendan T. McGann

***Abstract*—A new expression for the mean value of ocean surface sunglint, modeled as a binary-valued random process, is calculated. Multiple sunglint realizations are generated by applying the specular condition for particular viewing geometries to ocean surface elevations with Gaussian roughness spectra. The sunglint mean value is used to determine the relationship between the second-order statistics of the surface slope and sunglint random processes, and this relationship is successfully inverted to retrieve the slope autocorrelation and power spectrum from the simulated sunglint data. The inversion model is then applied to an image recorded coincident with the NASA AIRSAR PACRIM2 field campaign, to retrieve the 1-D elevation power spectrum.**

***Index Terms*—Inverse model, random processes, sunglint.**

I. Introduction

THE OCEAN and other natural water bodies arguably exhibit the most humanly recognizable example of wave motion present in nature. An understanding of the ocean's undulations and the underlying physical processes has applications to areas such as maritime and civil engineering, radar, and the remote sensing of bulk ocean characteristics, the measurement of which may be affected by the shape of the water surface. This being the case there is a long and varied history of attempts to characterize and understand the motions of the ocean surface.

The acquisition of ocean surface data has historically been pursued using *in situ* methods. Bottom-mounted pressure sensors, or accelerometers following the free surface, have been the traditional method of obtaining time series of the surface elevation, from which the frequency spectrum can be obtained. For the experimental situations for which pressure sensors and the like are appropriate, the gravity wave dispersion relation would be used to obtain the wavenumber spectrum. Such techniques can provide very direct measurements of the physical quantities of interest, but they are costly to build, deploy and operate, sample only a single location, and yield reasonable accuracy over only a limited band of wave frequencies.

In recent years, an emerging requirement for near-simultaneous, high spatial resolution observations over entire regions has focused attention on remote sensing technologies which can conduct measurements over vast swathes of ocean from airborne or spaceborne platforms. Both active and passive sensor systems have been developed, among the best known of which are methods which retrieve wavenumber spectra by imaging the surface in an extended spatial sense using photographic or video techniques.

Stereo photography is not only the oldest method of obtaining spatial measurements of the water surface, but it is also one of the most widely used [1], culminating in effort with the Stereo Wave Observation Project (SWOP) in 1954 [2]. In the SWOP experiment, pairs of photographs of a relatively large patch of ocean were taken by two aircraft, the cameras tripped simultaneously using a radio link. In [3] pairs of photographs were taken using a ship as the platform, with a 20×20 ft spatial area covered by each of the photographs.

Cox and Munk [4] used aerial photographs of ocean sunglint patterns to infer the surface wave slope probability density functions for a variety of conditions, the results of which are still in use today. The slope distribution was seen to be approximately Gaussian, and higher order corrections for skewness and kurtosis of the distributions were also given.

By optically analyzing an aerial photograph of the ocean [5], it was shown that the primary periodicities in the ocean scene could be identified in the diffraction pattern, as well as the primary direction of wave travel, and hence it was demonstrated that the photographic recording of ocean scenes was potentially a useful way of efficiently acquiring information about a large area of ocean.

Efforts to provide a more rigorous connection between images of the ocean surface and their corresponding wavenumber spectra have been made by several authors. A first-order theory was developed connecting the photographic and slope spectra, the latter from which the elevation spectrum could then be calculated [6], [7]. This theory was extended to second order, making explicit consideration of the various types of sky radiance distribution [8], [9].

In these attempts, it was vital that the distribution of sky radiance was monotonic (or at worst slowly varying), so that a unique and continuous relationship could be specified between the radiance reaching the camera and the wave slope. For this reason, it was pointed out that while images of sunglint had been proven to be useful in the determination of the slope probability distribution, they were of little utility in the measurement of wave spectra as they did not provide a continuous relationship between the detected radiance and the wave slope [6].

Alvarez-Borrego [10] presented a new method which was able to retrieve elevation spectra from sunglint data, by relating the glint and wave slope autocorrelations, thereby circumventing the discontinuous nature of sunglint images. However, it

Manuscript received October 17, 2005; revised April 3, 2006. This work was supported in part by the Curtin University of Technology and Defence Science and Technology Organisation.

G. P. Cureton, M. J. Lynch, and B. T. McGann are with the Department of Applied Physics, Curtin University of Technology, Perth, WA 6845, Australia (e-mail: geoff.cureton@physics.org).

S. J. Anderson is with the Defence Science and Technology Organisation, Salisbury, S.A., Australia (e-mail: stuart.anderson@dsto.defence.gov.au).

Digital Object Identifier 10.1109/TGRS.2007.900676

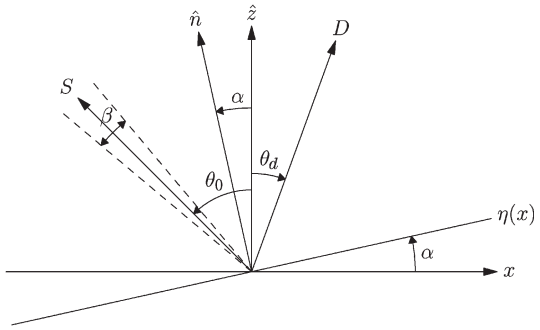

Fig. 1. Geometry of the experiment for the case where the specular condition is met.

is believed that an error was made in the calculation of the theoretical mean value of the glint data, which results in an incorrect theoretical relationship between the glint and slope autocorrelations, upon which the retrieval method is based.

In this paper, we describe the sunglint model given by [10], calculate the correct expression for the glint mean, and show that the slope and elevation autocorrelations and power spectra can be successfully retrieved from 1-D realizations of simulated sunglint data. We then apply the inversion model to a photographic image of sunglint obtained while the NASA Airborne Synthetic Aperture Radar (AIRSAR) PACRIM2 field campaign was underway, to retrieve the 1-D elevation power spectrum.

II. Forward Model

A. Experimental Geometry

We have a 1-D surface elevation $\eta(x)$ with variance σ_η^2. The slope of this surface is given by $M(x) = \tan\alpha$, with variance σ_M^2. The surface is illuminated by a source S with zenith angle θ_0 and angular subtense β (Fig. 1). The beam is reflected at the specular point, at which the surface normal $\hat{n}$ makes an angle α with the zenith, and reaches the detector D with zenith angle θ_d. The angular subtense of the detector is small enough to ensure that θ_d does not change appreciably with x.

As we move along the surface, we encounter slopes that either do or do not satisfy the specular condition. If we set the slope values that satisfy this condition to unity, and all others to zero, the slopes $M(x)$ are mapped to the binary process $L(x)$. For the case where the source S is a point source, $L(x)$ would consist of a series of delta functions, each for a slope M_0 which satisfies the specular condition. Since the source of interest, the sun, subtends a finite solid angle, there are a small range of slopes $M_0 \pm \Delta M/2$ that satisfy the specular condition. This results in the delta functions becoming rectangular peaks of finite extent (Fig. 2).

We would like to be able to find some connection between the surface elevation $\eta(x)$ and the binary process $L(x)$, the latter of which constitutes the experimental data. We do not have a continuous, functional relationship between these two quantities, so it is not feasible to try and construct some inversion scheme between $\eta(x)$ and $L(x)$. Despite the fact that the glint process is discontinuous, given a long enough record of data and/or a suitable density of glints, the glint autocorrelation can be approximated as a continuous and differentiable quantity.

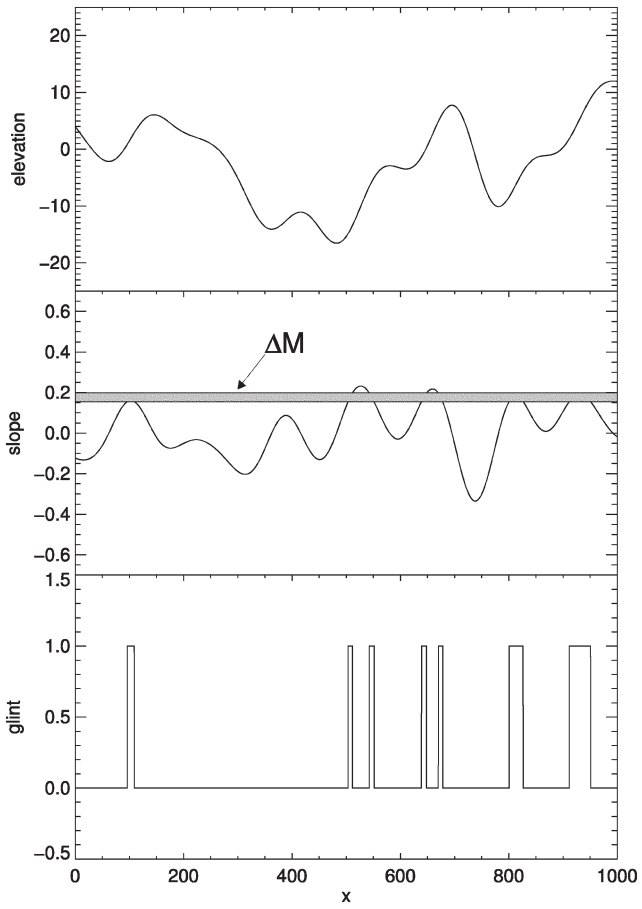

Fig. 2. Schematic representation (in arbitrary units) of the surface elevation $\eta(x)$, the surface slope $M(x)$ with the slope range ΔM selected by the glitter function, and the glint process $L(x)$.

Hence, it may be possible to find some connection between the glint and slope autocorrelations.

B. Glitter Function

In order to characterize the forward model, we must specify the way in which the surface slopes are transformed into the glint process $L(x)$. It is useful to think of the process as the operation of a filter $B(M)$, which acts upon the surface slopes. [10] determined the form of $B(M)$, which he called the glitter function.

In our case, the source is not a point source, but is extended, and this results in a finite range of slopes that will satisfy the specular condition. The transfer function $B(M)$ is a rectangular function centered on M_0, extending between $M_0 \pm \Delta M/2$. As a result, the glint process $L(x)$ will consist of a series of rectangular impulses of varying width, the width being dependent on the magnitude of the derivative of $M(x)$ in the vicinity of M_0.

Using geometric optical considerations, the glitter function was determined to be

$$B(M) = \mathrm{rect}\left[\frac{M - M_0}{(1 + M_0^2)\,(\beta/2)}\right] \tag{1}$$

which is a rectangular function with the range

$$M_- \leq M \leq M_+ \tag{2}$$

where

$$M_- = M_0 - \left(1 + M_0^2\right) \frac{\beta}{2} \tag{3}$$

$$M_+ = M_0 + \left(1 + M_0^2\right) \frac{\beta}{2}. \tag{4}$$

M_0 is the specular slope and β is the angle subtended by the source, in our case the Sun. Equation (2) has been derived in a more rigorous fashion [11], assuming a quasi-monochromatic, incoherent source of uniform intensity.

C. Relationship Between the Glint and Slope Autocorrelations

In defining the forward model, we require a connection between the measured quantity $L(x)$ and the surface slope $M(x)$.

Given that we have the random variable $L = L(x)$ with variance σ_L^2, we can take from L two further random variables $L_1 = L(x_1)$ and $L_2 = L(x_2)$. We may conclude also that L_2 is just L_1 which has been shifted by the amount $\tau = x_2 - x_1$. One quantity that we can calculate directly from $L(x)$ is the glint covariance $\sigma_L^2 C(\tau)$, which is related to $L(x)$ by

$$\begin{aligned}\sigma_L^2 C(\tau) &= \langle L_1 L_2 \rangle \\ &= \int\!\!\int_{-\infty}^{\infty} L_1 L_2 \, P_L(L_1, L_2) \, dL_1 \, dL_2\end{aligned} \tag{5}$$

where $P_L(L_1, L_2)$ is the joint probability of having glint values L_1 at x_1 and L_2 at x_2. Since $L(x)$ is a binary process, the integral in (5) can be replaced with

$$\sigma_L^2 C(\tau) = \sum_{i=0}^{1} \sum_{j=0}^{1} L_1^{(i)} L_2^{(j)} \, P_L\left(L_1^{(i)}, L_2^{(j)}\right) \tag{6}$$

where $L_1^{(i)} = i$ at position x_1, and $L_2^{(j)} = j$ at position x_2, and $P_L(L_1^{(i)}, L_2^{(j)})$ is the joint probability of $L(x)$ having values $L_1^{(i)}$ at x_1 and $L_2^{(j)}$ at x_2.

From (6), we can see that only one term in the summation is nonzero, for which $i = j = 1$. The glint covariance then becomes

$$\sigma_L^2 C(\tau) = L_1^{(1)} L_2^{(1)} \, P_L\left(L_1^{(1)}, L_2^{(1)}\right). \tag{7}$$

We can reasonably assume that the joint probability that there are glints at both x_1 and x_2 (i.e., $L_1 = L_2 = 1$) is just the joint probability that the slopes at these points are both within the range specified by the glitter function, i.e.,

$$\sigma_L^2 C(\tau) = \int\!\!\int_{M_-}^{M_+} L_1^{(1)} L_2^{(1)} P_M(M_1, M_2) dM_1 dM_2. \tag{8}$$

Noting that $L = B(M)$, we can write (8) as

$$\sigma_L^2 C(\tau) = \int\!\!\int_{-\infty}^{\infty} B(M_1) B(M_2) P_M(M_1, M_2) dM_1 dM_2 \tag{9}$$

which is the same as (4) in [10].

We are now left to specify the joint probability density of the random variables $M_1 = M(x_1)$ and $M_2 = M(x_2)$, with variances σ_M^2. Assuming that the surface slope is a zero-mean process, we have for $P_M(M_1, M_2)$ [12]

$$\begin{aligned}P_M(M_1, M_2) = &\frac{1}{2\pi\sigma_M^2 \sqrt{1 - Q^2(\tau)}} \\ &\times \exp\left[-\frac{M_1^2 - 2Q(\tau) M_1 M_2 + M_2^2}{2\sigma_M^2 \left[1 - Q^2(\tau)\right]}\right]\end{aligned} \tag{10}$$

where $Q(\tau)$ is the correlation of M_1 and M_2, and we have for the glint covariance

$$\begin{aligned}\sigma_L^2 C(\tau) = &\int\!\!\int_{-\infty}^{\infty} \frac{B(M_1) B(M_2)}{2\pi\sigma_M^2 \sqrt{1 - Q^2(\tau)}} \\ &\times \exp\left[-\frac{M_1^2 - 2Q(\tau) M_1 M_2 + M_2^2}{2\sigma_M^2 \left[1 - Q^2(\tau)\right]}\right] dM_1 dM_2.\end{aligned} \tag{11}$$

If we integrate over M_1, we get

$$\begin{aligned}\sigma_L^2 C(\tau) = &\frac{1}{\sqrt{8\pi\sigma_M^2}} \int_{-\infty}^{\infty} B(M_2) \left[\operatorname{erf}(\xi_+) - \operatorname{erf}(\xi_-)\right] \\ &\times \exp\left[-\frac{M_2^2}{2\sigma_M^2}\right] dM_2\end{aligned} \tag{12}$$

where

$$\xi_+ = \frac{M_+ - Q(\tau) M_2}{\sqrt{2\sigma_M^2 \left[1 - Q^2(\tau)\right]}} \qquad \xi_- = \frac{M_- - Q(\tau) M_2}{\sqrt{2\sigma_M^2 \left[1 - Q^2(\tau)\right]}}.$$

D. Relationship Between the Glint and Slope Variances

In order to normalize the glint covariance (12), we need to calculate the glint variance

$$\sigma_L^2 = \int_{-\infty}^{\infty} \left[B(M) - \mu_L\right]^2 P_M(M) dM \tag{13}$$

where the glint mean μ_L is

$$\mu_L = \int_{-\infty}^{\infty} B(M) P_M(M) dM \tag{14}$$

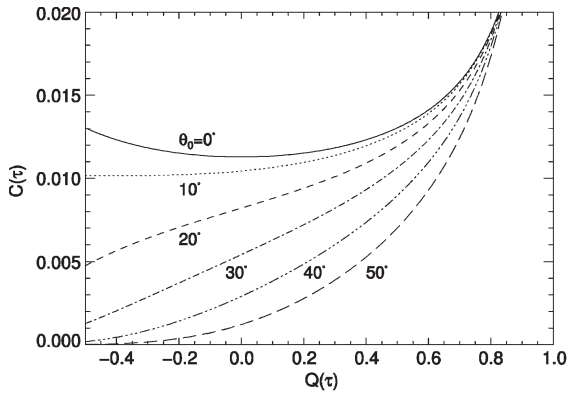

Fig. 3. Theoretical relationships between $C(\tau)$ and $Q(\tau)$, for several solar zenith angles.

and

$$P_M(M) = \frac{1}{\sqrt{2\pi\sigma_M^2}} \exp\left[-\frac{M^2}{2\sigma_M^2}\right]. \tag{15}$$

Expanding (13), we have

$$\sigma_L^2 = \int_{-\infty}^{\infty} \left[B^2(M) - 2B(M)\mu_L + \mu_L^2\right] P_M(M) dM.$$

Noting that $B^2(M) = B(M)$, we can write the glint variance in terms of the glint mean

$$\sigma_L^2 = \mu_L \left(1 - \mu_L\right) \tag{16}$$

where we calculate μ_L as

$$\mu_L = \frac{1}{2}\left[\operatorname{erf}\left(\frac{M_+}{\sqrt{2}\sigma_M}\right) - \operatorname{erf}\left(\frac{M_-}{\sqrt{2}\sigma_M}\right)\right]. \tag{17}$$

III. Inverse Model

As we have seen in the previous section, the expression for $C(\tau)$ is specified by (12), (16), and (17), respectively. Given that we can experimentally measure μ_L, σ_L^2, and $C(\tau)$, we are left to use this information, along with (12), (16), and (17), to retrieve σ_M^2 and $Q(\tau)$.

The slope variance σ_M^2 is retrieved by fitting the curve given by (17) to the measured values of the glint mean μ_L, with σ_M^2 as a fitting parameter.

Once we have retrieved the slope variance, we can use it in (12) to calculate the theoretical relationship between $C(\tau)$ and $Q(\tau)$, for the variances σ_L^2 and σ_M^2. Shown in Fig. 3 is the theoretical relationship between $C(\tau)$ and $Q(\tau)$ for the case of $\sigma_M = 0.2121$ for several values of θ_0, $\theta_d = 0^\circ$, and the glint mean given by (17). For the given slope and glint variances, the curves in Fig. 3 correspond to the ideal relationship between $C(\tau)$ and $Q(\tau)$.

For a particular solar zenith angle, the slope autocorrelation $Q(\tau)$ is retrieved by stepping through the glint autocorrelation values $C(\tau)$ for each value of τ, and using the correct curve in Fig. 3 to find the corresponding value of $Q(\tau)$. We can see that, for example, the case of $\theta_0 = 0^\circ$ is ill-posed, in that the inverse relationship between the glint and slope autocorrelations is multivalued for this particular geometry. In such a case, a different geometry, for which the inverse relationship was single valued, would need to be used.

Once we have the retrieved slope autocorrelation, the elevation autocorrelation is obtained using the relationship [13]

$$\sigma_M^2 Q(\tau) = -\sigma_\eta^2 \frac{d^2 R(\tau)}{d\tau^2}. \tag{18}$$

A Fourier transformation is then used to convert this to the elevation power spectrum $\Psi(k)$.

TABLE I
Theoretical, Simulated, and Retrieved Glint Means μ_L for Several Solar Zenith Angles θ_0. The Retrieved Slope Standard Deviation Is $\sigma_M = 0.2126$, Where the Original Value Was $\sigma_M = 0.2121$

θ_0	μ_L(theory)	μ_L(simulated)	μ_L(retrieved)
0°	0.011 161	0.011 112	0.011 109
10°	0.010 329	0.010 290	0.010 297
20°	0.008 146	0.008 132	0.008 141
30°	0.005 386	0.005 402	0.005 398
40°	0.002 900	0.002 917	0.002 912
50°	0.001 212	0.001 211	0.001 218

IV. Simulations

A series of simulations were performed to test the retrieval of σ_M^2 and $Q(\tau)$. To this end, 10 000 surface elevation realizations $\eta(x)$ were generated, with each surface having 65 536 points, $\Delta x = 0.2$ cm, $\sigma_\eta = 13$ cm, the power spectrum

$$\Psi(k) = \sqrt{l^2\pi}\sigma_\eta^2 \exp\left[-\frac{l^2k^2}{4}\right] \tag{19}$$

and the correlation length

$$l = \frac{\sqrt{2}\sigma_\eta}{\sigma_M}. \tag{20}$$

The correlation length was adjusted such that the resulting slope realizations had the standard deviation $\sigma_M = 0.2121$.

The forward glint model, as represented by the glitter function (1), was applied to the slope realizations $M(x)$ to produce multiple glint realizations $L(x)$, for the solar zenith angles $\theta_0 = 10^\circ, 20^\circ, 30^\circ, 40^\circ$, and 50°. A detector zenith angle $\theta_d = 0^\circ$ was used. Realization averaged glint autocorrelations and variances were calculated from the glint realizations for each solar zenith angle.

Shown in Table I are the theoretical, simulated, and retrieved glint means, for each solar zenith angle. We can see that there is good agreement between the simulated and theoretical glint means, where the theoretical values were calculated using (17). We also note that the retrieved slope standard deviation of

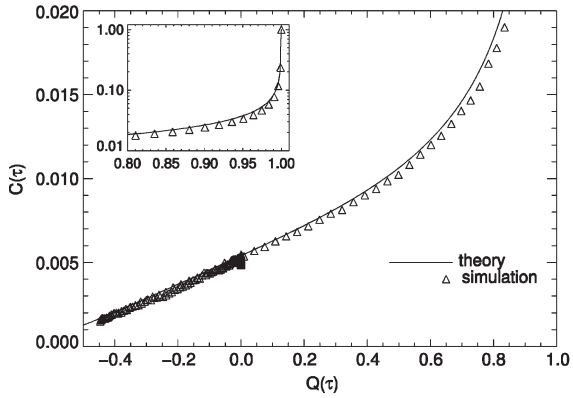

Fig. 4. Theoretical and simulated relationships between $C(\tau)$ and $Q(\tau)$, for $\theta_0 = 30°$.

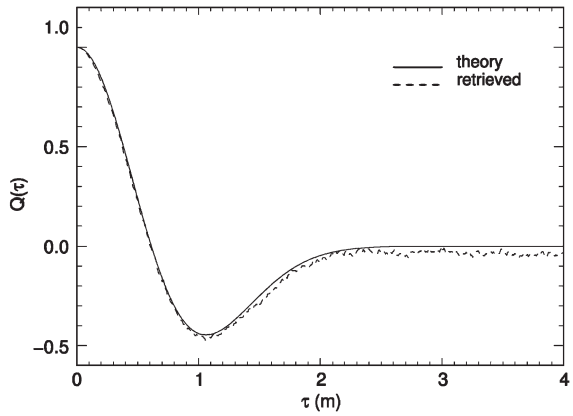

Fig. 5. Theoretical and retrieved slope autocorrelations $Q(\tau)$.

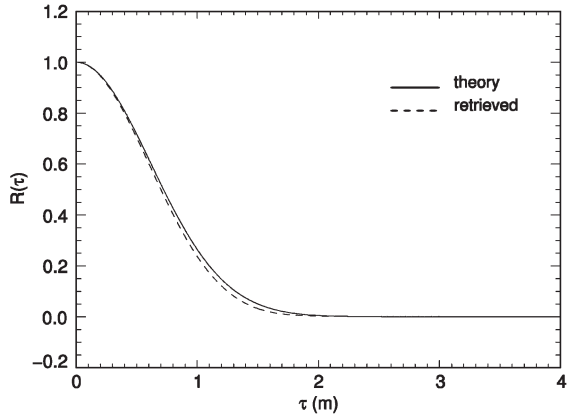

Fig. 6. Theoretical and retrieved elevation autocorrelations $R(\tau)$.

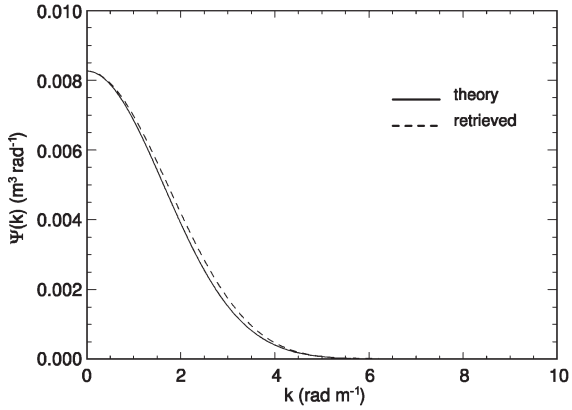

Fig. 7. Theoretical and retrieved elevation power spectra $\Psi(k)$.

$\sigma_M = 0.2126$ is in good agreement with the original value $\sigma_M = 0.2121$.

In Fig. 4 is the theoretical relationship (12) between the glint and slope autocorrelations (solid line), using the simulated μ_L and retrieved σ_M from Table I, for $\theta_0 = 30°$. Also shown (triangles) is the relationship between the simulated glint autocorrelation and the theoretical slope autocorrelation. While the comparison between these two curves would not be possible in actual experimental conditions, in this simulation exercise, it provides a useful way of quantifying the way in which the variability in the simulated (measured) glint mean, and in the retrieved slope variance, affect the quality of the retrieval. The simulated data generally fall below the theoretical curve, and as a result there will be a negative bias of the retrieved slope autocorrelation as τ approaches infinity. This effect is most pronounced where the $C(\tau) - Q(\tau)$ gradient is the smallest, in that a small perturbation in the value of $C(\tau)$ results in a large change in the value of $Q(\tau)$. It is for this reason that this value of θ_0 was chosen, as it has a steeper gradient overall in the critical range $-0.4 \leq Q(\tau) \leq 0.8$.

Shown in Figs. 5–7 are the theoretical and retrieved slope autocorrelations, elevation autocorrelations, and elevation power spectra, respectively. We observe that for each of these quantities, the theoretical and retrieved curves are in good agreement. However, in Fig. 5, we can see that for large τ the retrieved $Q(\tau)$ does not tend to zero, but to some finite amount. This is a direct consequence of the variability in the theoretical $C(\tau) - Q(\tau)$ relationship, which has σ_L^2 and σ_M^2 as input parameters. This highlights the need for the accurate determination of the glint variance and autocorrelation, and hence the slope variance.

Since both the elevation and slope power spectra for a realistic ocean surface would be bandlimited, we expect that the corresponding autocorrelations would show similar behavior. Specifically, $Q(\tau)$ and $R(\tau)$ should tend to zero in the limit of large τ. To ensure that the retrieval satisfied this requirement, a Butterworth lowpass filter was applied to the slope autocorrelation, and the filter cutoff was adjusted until $R(\tau)$ and $R'(\tau)$ approached zero for large τ.

In this paper, we have examined the sunglint retrieval model presented in [10], and we have seen that it is successful in retrieving elevation wavenumber power spectra from glint data. However, we believe that the original model as published contained an error in the calculation of the glint mean μ_L. Here, we have calculated this quantity to be given by (17), whereas (4) of [14] specified the glint mean as

$$\mu_L = \operatorname{erf}\left(\frac{M_+}{\sigma_M}\right) - \operatorname{erf}\left(\frac{M_-}{\sigma_M}\right). \tag{21}$$

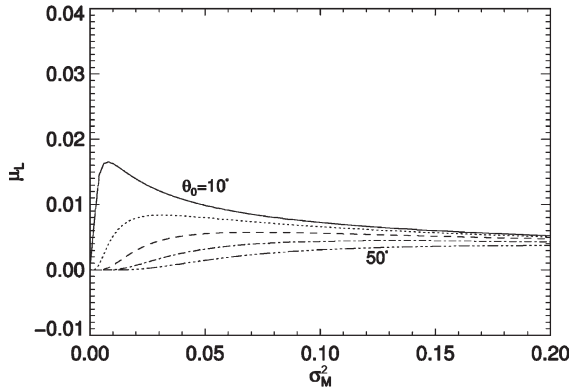

Fig. 8. Theoretical relationship between the glint mean and slope variance (17), for several solar zenith angles.

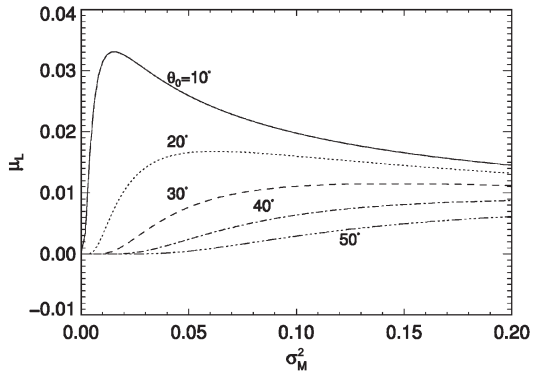

Fig. 9. Theoretical relationship between the glint mean and slope variance (21), for several solar zenith angles.

Shown in Figs. 8 and 9 are the relationships between the glint mean μ_L and slope variance σ_M^2 for several solar zenith angles, where μ_L is given by (17) and (21), respectively. We can see that for the slope standard deviation used both in this paper and by Alvarez-Borrego ($\sigma_M = 0.2121$), (21) overestimates the glint mean for the smaller solar zenith angles, and underestimates for the larger solar zenith angles.

V. Beagle Gulf Experiment

The sunglint inversion model described above was applied to imagery obtained in a Defence Science and Technology Organisation (DSTO) experiment in Beagle Gulf, north of Darwin, attached to the NASA AIRSAR PACRIM2 field campaign. The images were obtained from a helicopter using a digital camera, for 12 azimuth angles and several detector heights. Shown in Fig. 10 is the experimental geometry used. We now have the 2-D surface elevation $\eta(x, y)$ with variance σ_η^2. The slope of this surface is given by $M_x(x, y)$ and $M_y(x, y)$, with variances $\sigma_{M_x}^2$ and $\sigma_{M_y}^2$, respectively. The surface is illuminated by a source S with zenith angle θ_s, azimuth angle ϕ_s and angular subtense β. The beam is reflected at the specular point, at which the surface normal $\hat{n}$ makes an angle θ with the zenith, and reaches the detector D with angles θ_d and ϕ_d.

Because we are now dealing with a 2-D geometry, we must alter our definition of the specular slope to include the

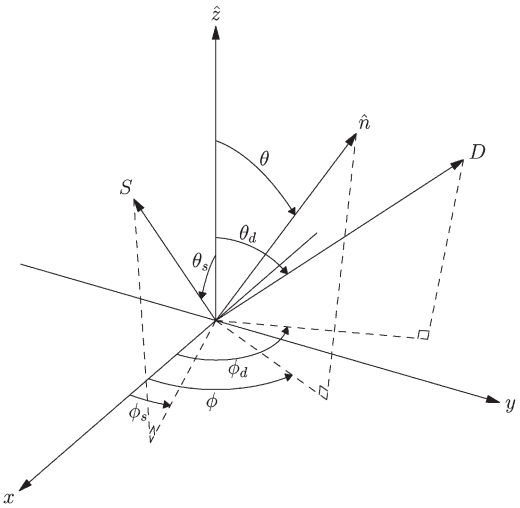

Fig. 10. Geometry of the specular reflection of sunlight from the ocean surface.

azimuthal variation of S and D, so we are able to use our 1-D retrieval model. If we now apply our 1-D model along the x-direction, the x-component of the specular slope is

$$M_{0x} = \frac{\sin\theta_s \cos\phi_s + \sin\theta_d \cos\phi_d}{\cos\theta_s + \cos\theta_d}. \tag{22}$$

In this paper, the x-axis was taken to be along the plane of the detector and the specular point, and as such we had $\phi_d = 0°$. Shown in Fig. 11 are the original, scaled and clipped images for the angles $\theta_d \approx 34°$, $\theta_s \approx 26°$, and $\phi_s \approx 165°$, and a detector height of approximately 300 m. The extent of the glint data along the x-direction (along the columns of the image) was approximately 190 m, and the subtense of the detector along this direction was approximately $24°$.

If we examine the original image [Fig. 11(a)], we can see that there is relatively little contrast. This is due to the significant level of upwelling optical radiation, reflected from the shallow bottom present in Beagle Gulf. To facilitate the distinction between glint features and bottom reflection, the image was histogram equalized to produce Fig. 11(b). The process of equalization attempts to balance the levels of occupancy of the various gray levels in the image, thereby increasing the contrast between features in an image, which would otherwise have similar image intensities. In this way, we hope to reduce the erroneous identification of bright pixels as glint events. We then clip the equalized image to produce the binary image in Fig. 11(c).

Once we obtained the binary image, the glint autocorrelation and variance were calculated for each column of the image, and averaged to reduce the effects of statistical noise. The glint variance was found to be $\sigma_L^2 = 0.0038$, from which a slope standard deviation of $\sigma_M = 0.16$ was retrieved. The glint and retrieved slope variances, and the glint autocorrelation were used in the sunglint model to retrieve the slope autocorrelation, elevation autocorrelation, and elevation power spectrum, for the column direction of the image, all of which are shown in

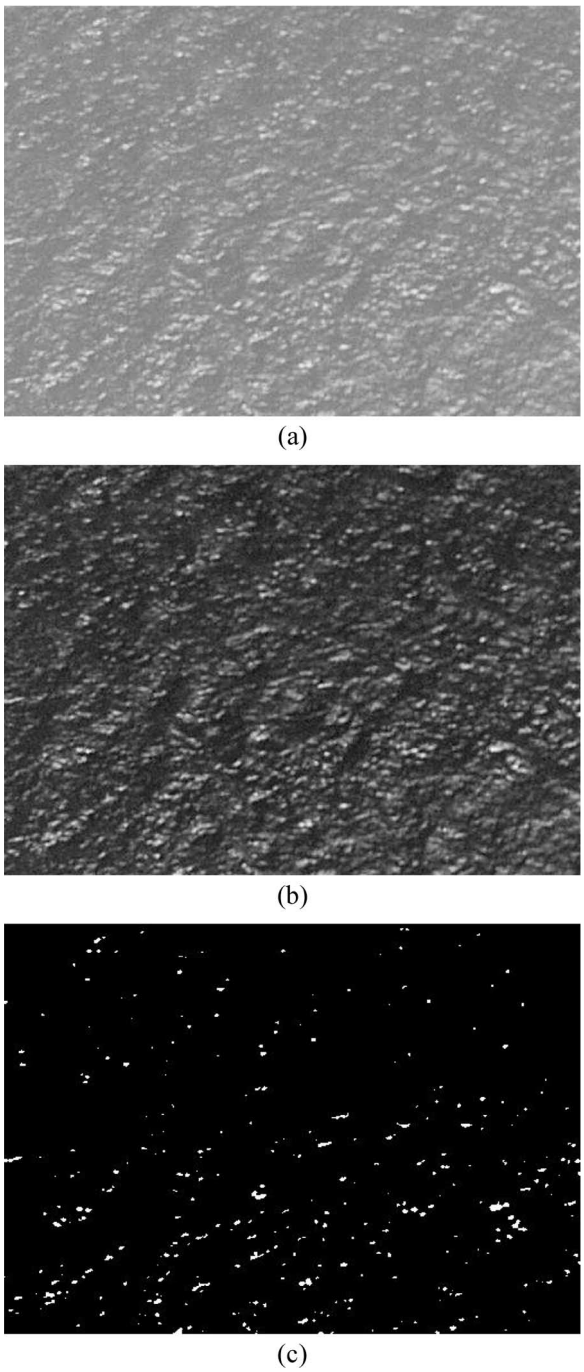

(a)

(b)

(c)

Fig. 11. Shown in this figure are the (a) original, (b) scaled, and (c) clipped images of the ocean surface in Beagle Gulf. The distance along the columns of the images is approximately 190 m.

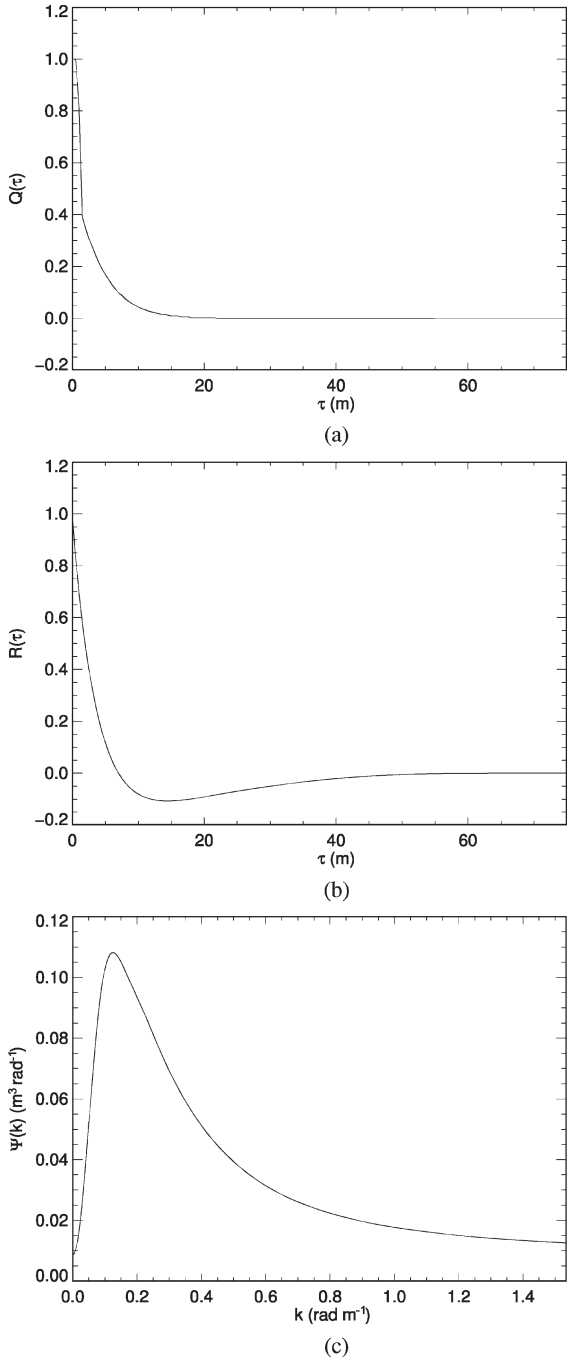

Fig. 12. Shown in this figure are the retrieved (a) slope and (b) elevation autocorrelations, and (c) the retrieved elevation power spectrum, corresponding to the images in Fig. 11.

Fig. 12. We note that the elevation power spectrum [Fig. 12(c)] is similar in form to the Pierson–Moskowitz spectrum, which is typical of oceanic wind waves. The spatial increment was estimated to be approximately 0.5 m, and as such the retrieved elevation variance was determined to be approximately $\sigma_\eta^2 = 0.2\ \mathrm{m}^2$.

VI. Conclusion

In this paper, we have calculated a new expression for the mean of the sunglint random process. This allowed us to determine the correct relationship between the glint and slope statistics, which was successfully inverted to determine the slope and elevation autocorrelations and power spectra from simulated 1-D sunglint data. The sensitivity of the retrieval process was examined with respect to variations in the retrieved value of the slope variance. Such variations resulted in the retrieved slope autocorrelation tending to a finite value for large lag, which is aphysical. A Butterworth lowpass filter was applied to the retrieved slope autocorrelation, the specific form of the filter being chosen so that the elevation autocorrelation and its derivatives vanish for large values of the lag. The 1-D

inversion model was then applied to an image of sunglint, and the elevation power spectrum for the column direction of the image was successfully retrieved.

An inherent limitation of the retrieval model considered in this paper, and indeed any retrieval method based on second-order statistics, is that any phase information about the random surface is lost. One consequence is that we are unable to determine the direction of wave travel, and we have no information about the interactions between wave spectral components. To alleviate this deficiency, we propose to generalize the model described here to retrieve higher order statistical quantities, namely the slope and elevation bispectra, which are dependent on the skewness of these quantities. In addition to removing the π radian ambiguity in the retrieved direction of wave travel for moderately nonlinear surface waves (for example those present in shallower coastal waters), this would allow the determination of the relative contributions to the wave spectral components of spontaneous excitation and nonlinear coupling.

ACKNOWLEDGMENT

The authors would like to thank Dr. J. Alvarez-Borrego for the provision of preprints, software, and some useful discussions regarding his sunglint inversion model, and DSTO for coordinating the aerial photography and associated buoy deployments.

REFERENCES

[1] B. Jähne, J. Klinke, and S. Waas, "Imaging of short ocean waves: A critical theoretical review," *J. Opt. Soc. Amer.*, vol. 11, no. 8, pp. 2197–2209, 1994.

[2] L. Cote, J. Davis, W. Marks, R. McGough, E. Mehr, W. Pierson, Jr., J. Ropek, G. Stephenson, and R. Vetter, "The directional spectrum of a wind generated sea as determined from data obtained by the stereo wave observation project," *Meteorol. Pap.*, vol. 2, no. 6, pp. 395–400, 1960.

[3] E. B. Dobson, "Measurement of the fine-scale structure of the sea," *J. Geophys. Res.*, vol. 75, no. 15, pp. 2853–2856, 1970.

[4] C. Cox and W. Munk, "Measurement of the roughness of the sea surface from photographs of the sun's glitter," *J. Opt. Soc. Amer.*, vol. 44, no. 11, pp. 838–850, 1954.

[5] N. F. Barber, "A diffraction analysis of a photograph of the sea," *Nature*, vol. 164, p. 485, 1949.

[6] D. Stilwell, Jr., "Directional energy spectra of the sea from photographs," *J. Geophys. Res.*, vol. 74, no. 8, pp. 1974–1986, 1969.

[7] D. Stilwell, Jr. and R. O. Pilon, "Directional spectra of surface waves from photographs," *J. Geophys. Res.*, vol. 79, no. 9, pp. 1277–1284, 1974.

[8] R. S. Kasevich, "Directional wave spectra from daylight scattering," *J. Geophys. Res.*, vol. 80, no. 33, pp. 4535–4541, 1975.

[9] N. A. Peppers and J. S. Ostrem, "Determination of wave slopes from photographs of the ocean surface: A new approach," *Appl. Opt.*, vol. 17, no. 21, pp. 3450–3458, 1978.

[10] J. Alvarez-Borrego, "Wave height spectrum from sunglint patterns: An inverse problem," *J. Geophys. Res.*, vol. 98, no. C6, pp. 10 245–10 258, 1993.

[11] J. Alvarez-Borrego, "1-D rough surfaces: Glitter function for remote sensing," *Opt. Commun.*, vol. 113, no. 4, pp. 353–356, Jan. 1995.

[12] W. B. Davenport, Jr. and W. L. Root, *Random Signals and Noise*. New York: McGraw-Hill, 1958.

[13] A. Papoulis, *Probability, Random Variables and Stochastic Processes*. New York: McGraw-Hill, 1965.

[14] J. Alvarez-Borrego, "Some statistical properties of surface heights via remote sensing," *J. Mod. Opt.*, vol. 42, no. 2, pp. 279–288, 1995.

Geoff P. Cureton received the B.Sc. degree (Honours) in physics, studying error propagation in the ill-posed retrieval of aerosol size distributions from radiometric data, from the Curtin University of Technology, Perth, Australia, in 1997, where he is currently working toward the Ph.D. degree, studying the retrieval of polyspectra from nonlinear ocean surfaces using sunglint within the Remote Sensing and Satellite Research Group.

Other research interests include the simulation of nonlinear surfaces and stochastic processes in remote sensing of the ocean.

Stuart J. Anderson received the B.Sc. and Ph.D. degrees in physics from the University of Western Australia, Perth, in 1968 and 1972, respectively, before joining the Defence Science and Technology Organisation team assembled to develop the Jindalee over-the-horizon radar system.

He has worked as a Visiting Scientist in the U.S., U.K., and France, and has lectured widely on topics related to HF radar. He maintains close links with the Curtin University of Technology, where he is an Adjunct Professor of applied physics. Currently, his active interests include adaptive signal processing, electromagnetic scattering from random surfaces, structure and dynamics of small-scale ionospheric irregularities, radar polarimetry, and the design of HF radar systems for a wide variety of missions.

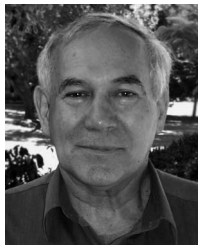

Mervyn J. Lynch received the B.Sc. (Honours) and Ph.D. degrees in physics, studying electronic spectroscopy of solids, from the University of Western Australia, Perth, in 1964 and 1971, respectively.

He was a Postdoctoral Fellow at the J. J. Thomson Laboratory, University of Reading, in 1971–1973, researching the photoelectron spectroscopy and photoabsorption cross sections of noble gases and atmospheric trace gas species using synchrotron radiation. He has been a faculty member of the Department of Applied Physics, Curtin University of Technology, Perth, Australia, where he established the Remote Sensing and Satellite Research Group. His research has focused on remote sensing science, including radiative transfer, inverse methods, algorithm development, and validation of atmospheric, ocean, and land geophysical products from satellites, including AVHRR, SeaWiFS, ATSR2, MODIS, GLI, and MERIS.

Brendan T. McGann received the B.Sc. (Honours) and Ph.D. degrees in physics, studying HF radar oceanography, from the James Cook University of North Queensland, Townsville, Australia, in 1980 and 1987, respectively.

He was a Postdoctoral Fellow at University College Galway, University of Ireland, in 1987–1988, researching the below-cloud scavenging of atmospheric aerosols. He has worked as a Research Scientist for Defence Science and Technology Organisation, Salisbury, S.A., investigating anomalous tropospheric propagation of HF radio waves. Since 1990, he has been a faculty member of the Department of Applied Physics, Curtin University of Technology, Perth, Australia, where he has conducted oceanographic research for the Centre for Marine Science and Technology, and remote sensing research with the Remote Sensing and Satellite Research Group. His research has focused on remote sensing science, including radar altimetry, ocean color, and algorithm development for sediment concentration using MODIS and MAS.